sciendo

LATVIAN JOURNAL OF PHYSICS
AND TECHNICAL SCIENCES
2024, N 5

DOI: 10.2478/lpts-2024-0032

SYNTHESIS OF PERIODIC POROUS STRUCTURES ON THE SURFACE OF INDIUM PHOSPHIDE

Y. Suchikova[1*], S. Kovachov[1], I. Bohdanov[1], M. Konuhova[2], A. I. Popov[2]

[1] Berdyansk State Pedagogical University,
4 Schmidt Str., Berdyansk, 71100, UKRAINE
[2] Institute of Solid State Physics,
University of Latvia,
8 Kengaraga Str., Riga, LV-1063, LATVIA
*e-mail: yanasuchikova@gmail.com

The paper demonstrates the possibility of forming specific nanostructures of the "parquet" type of nanowires on the InP surface. The resulting nanostructure is characterised by an ordered transverse and longitudinal relative shift of separate nanowires. A dislocation model is proposed that explains the mechanism of such structure formation. The numerical estimates of the geometric parameters of the nanostructure obtained during theoretical modelling are quite adequate for the experimental results.

Keywords: *Dislocations, electrochemical etching, indium phosphide, periodic nanostructures, porous oxide.*

1. INTRODUCTION

The interest in nanostructured semiconductors is due to the variety of morphological forms obtained [1], [2] and the broad prospects for applications [3]–[14]. Today, many different methods of surface nanostructuring are known, including the method of reactive magnetron sputtering [15], matrix synthesis [16], electrochemical deposition [17], [18], electrochemical etching [19], [20], lithography [21], etc. Electrochemical etching is increasingly popular due to the simplicity of technology and low cost [22]. This method has shown the highest efficiency for the nanostructuring of Si and A_3B_5 semiconductors, in particular, InP, GaP, GaAs [23]–[25]. When these semiconductors are etched in selective etchants, etching holes are often observed on the surface and in most of the crystal [26], [27]. A high concentration of etching pits determines the porous structure of the semiconductor plate, which causes a change in

properties and has been widely used. In particular, as a result of the high surface roughness, the range of light absorption expands, making it possible to use such structures as a material for PEP [28]. When the resistivity of porous structures is increased, an improvement in piezoelectric characteristics is observed, which is promising for the creation of sensors [29]. Porous semiconductors are known to be applied as a template for nanorods and nanotubes [30]. Porous layers are a 'soft' substrate for growing thin films, in particular, InN, GaN, etc. [31]. A promising direction is now directed controlled electrochemical etching, which leads to the formation of ordered periodic nanostructures [32].

As a rule, the formation of pores during electrochemical etching of a semiconductor begins at the sites of localisation of crystal lattice defects [33], [34]. This process can be accompanied by alternative reactions, for example, the formation of continuous insoluble films, surface texturing, overgrowing with oxides, etc. [35]–[38]. This is the reason for the low controllability of the process and the lack of a single mechanism for the pore formation process on the semiconductor surface.

In this study, the formation of periodic porous structures on the surface of n-InP (111) is reported, the mechanisms of their formation and their chemical composition are investigated.

2. EXPERIMENTAL DETAILS AND RESULTS

The structures were formed by electrochemical etching in a hydroalcoholic solution of hydrofluoric acid $HF:H_2O:C_2H_5OH=1:1:2$ at a constant current density $j=150$ mA/cm^2. A simple electrochemical cell with platinum on the cathode was used for etching. The experiment was carried out in the dark at room temperature. Before the experiment, the samples were cleaned with alcohol and vinegar. After electrochemical etching, the samples were kept in the same electrolyte for 10 minutes. The technology is described in detail in our work [19], [34]. The electrolyte was stirred during etching in order to remove bubbles from the semiconductor plate.

The morphological characteristics of the produced nanostructures were investigated using scanning electron microscopy. Chemical analysis of the surface layers was performed using the EDAX and INCA energy methods.

As a result of etching, structures were obtained in the form of massive porous nanowires packed according to the "parquet" type (Fig. 1a). The thickness of each wire is about 10 microns, the height is up to 10 microns, and the length is between 100 and 130 microns. The distance between the parquet layers is 20 to 50 microns. The wires have a porous, loose structure. They peel off easily from the crystal surface. Also, on closer inspection, one can notice that the parquet areas are easily combined with each other. In Fig. 1b, one can see a nanowire that broke at a cleavage of the crystalline material. This shows the fragility and looseness of the structure. In addition, an uneven crater structure of the surface of the InP sample is observed.

According to the results of the chemical analysis of the surface layers, the wires contain oxygen (Table 1), showing the formation of the oxide phase.

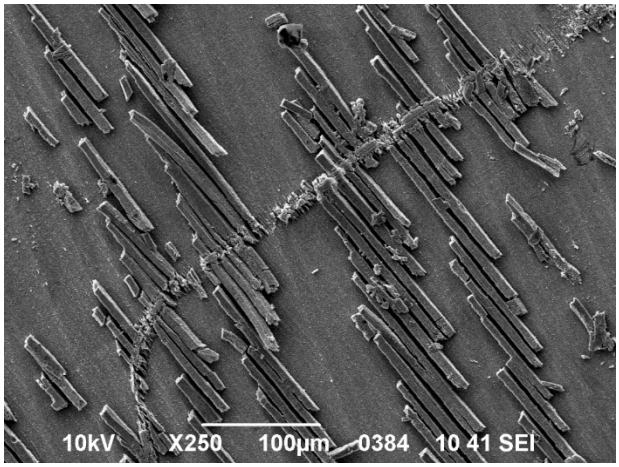

a)

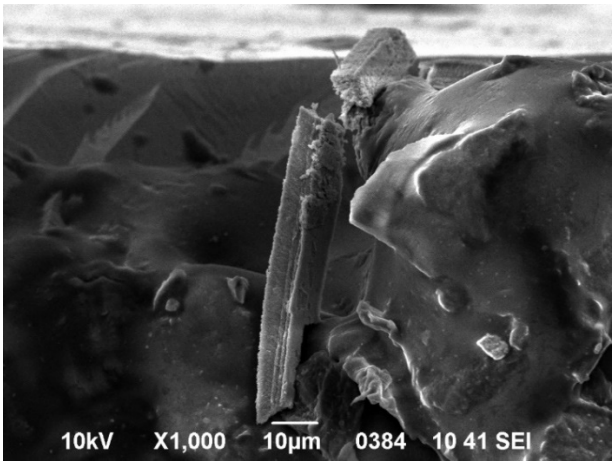

b)

Fig. 1. SEM image of the InP: a) surface after electrochemical etching in an hydroalcoholic solution of hydrofluoric acid; b) cleavage with a broken wire.

Table 1. Chemical Analysis of Surface Layers

Point of the surface	Element			Total
	O	P	In	
a	18.70	11.04	70.26	100.00
b	16.09	8.71	75.20	100.00
c	14.56	10.92	74.52	100.00
d	18.05	3.1	78.85	100.00
Average value	16.85	8.44	74.71	100.00

There are small concentrations of phosphorus (on average 8.44 %) and oxygen (on average 16.85 %), while indium is present in high concentrations (on average 74.71 %).

3. DISCUSSION

3.1. Electrochemical Processes on the Surface of Indium Phosphide in an Electrolyte Solution

In the interaction of A^3B^5 compounds with acid solutions, it is necessary to take into account the nature and chemical properties of the individual elements that are parts of the compound, as well as the physicochemical properties of the surfaces of the compounds. Since In and P elements are representatives of different groups, they are amenable to the action of oxidising agents. This is because of the nature of their redox properties. The component with the lower redox potential will oxidise first. At the same time, to maintain electroneutrality, the second component will pass into the solution simultaneously with it. Since the standard electrode potential of group III elements has a negative value and lower values of the potential of group V elements, In will be oxidised first. It should be noted that indium is characterised by moderate chemical activity and is resistant to water and air. During the electrolytic treatment of InP in a hydrofluoric acid solution, in the first stages of etching, a dense oxide film is formed, presumably of In_2O_3 oxide with $InPO_3$ inclusions. On the other hand, phosphorus reacts better with electrolyte anions, so its sublattice is etched faster. With an already formed In_2O_3 film, an interaction takes place between oxide and phosphorus diffusing from the bulk of the crystal, which can lead to the release of free indium, metallization of the growing layer on the crystal surface, and removal of phosphorus into the electrolyte solution. As a result, there is an excessive content of indium in the oxide layers.

It is obvious that the crystal lattices of indium phosphide and oxide have a significant mismatch. This leads to an appearance of excess stress. In addition, the film is loosely adhered to the substrate. As a result, we observe delamination and "spread" of the film upon further etching of the sample.

In_2O_3 is quite resistant to dilute acids; however, the current forms pores on its surface, it becomes soft and fragile (which is well demonstrated in Fig. 1b).

It is not the chaotic spreading of the oxide film that seems interesting, but the formation of even parallel steps equidistant from each other. In addition, there is a longitudinal uniform displacement of adjacent steps relative to each other. It is possible that such a periodicity of the structures is due to the concentration inhomogeneity of the impurity distribution in the bulk of indium phosphide. When a crystal uses the Czochralski method, a peculiarity of the distribution of the main (In, P) and minor (S) components is observed. In the direction from the centre to the periphery, the concentration of charge carriers increases, and their mobility decreases (a consequence of the temperature gradient). In addition, long-range elastic mechanical stresses prevent the formation of concentration and geometrically homogeneous single crystal. The sources of these mechanical stresses are dislocations (and their multiplication), which arise at internal growth defects. As a result, the crystal has a banded internal structure, in which areas with normal and high levels of dopant impurity concentration alternate.

When such a crystal is etched, areas with an increased concentration of impurities will be etched out faster. As a result, they will be very porous and have a low

phosphorus content. These areas are the initial sources of the formation of the oxide film. In these areas, the oxide layer has the greatest adhesion to the surface. This explains the sticking of oxide steps in the bands of segregation inhomogeneity.

3.2. The Mechanism of Formation of the Periodic Structure

Let us consider in detail a possible mechanism for the formation of a periodic structure of defects near or on the sample surface. As an initial hypothesis, we will accept the assumption that the geometric shape of such a structure is identical to the shape of the surface "parquet" structure.

The sample surface coincides with the crystal face (111). In this case, the faces of conservative slip of edge dislocations for the cubic crystal structure of sphalerite (InP) are located towards the sample surface, as shown schematically in Fig. 2.

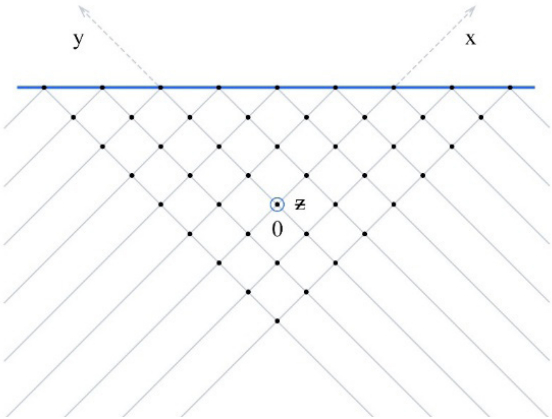

Fig. 2. Slip faces of edge dislocations in a cubic crystal structure.

Let us assume that at a sufficient distance from the surface (comparable to the sample thickness) there is a source of rectangular dislocation loops. The mechanism of operation of this source of dislocation loops is described in detail in [36]. The sliding system of these loops is a lateral surface of a prism composed of crystal planes (101), (110) (Fig. 3a).

As a result of repulsive interaction, the loops will spread along the sliding system from the source to the opposite surface of the sample. We will call the first loop (the most distant from the source) the "head" one, the next one – "upcoming". The movement of the loops will stop after one of the sides of the head loop comes out onto the surface of the sample (Fig. 3b). A step is formed on the sample surface, and the other three dislocations forming the loop will be fixed. As a result, the following (upcoming) dislocation loops will stop moving in the slip system and form a cluster.

Before the emergence of the head dislocation loop on the sample surface, the relative position of the head and the upcoming loops is symmetric toward the [010] and [001] directions (the OY and OZ axes). As a result, the superposition of the components of the Peach-Keller forces affecting the sections of the incident dislocation loop from the side of the stress field of the head dis-

location loop will be zero for all directions, except for [100] (the OX axis). This means that until the head dislocation loop emerges on the surface, the upcoming loop will not shift along the OY and OZ axes (Fig. 3a).

After the head dislocation loop emerges on the surface, the symmetry of the mutual arrangement of the upcoming and head dislocation loops will be broken. As a result, it will become possible to displace the upcoming dislocation loop along the OY axis (Fig. 3a).

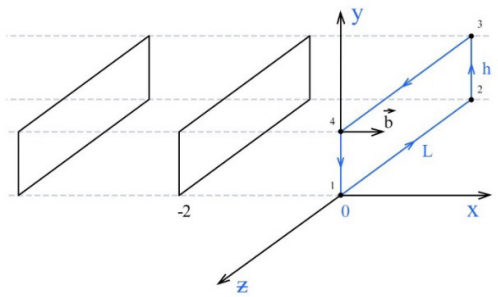

a)

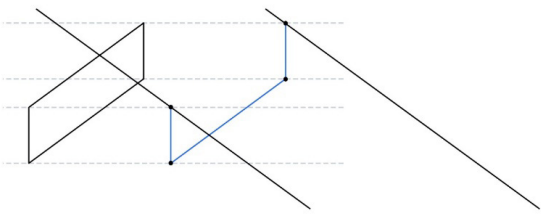

b)

Fig. 3. Rectangular dislocation loops (a) and fixation of the head dislocation loop of a cluster on the sample surface (b).

Let us apply the expression for the components of the Peach-Keller force affecting per unit length of the dislocation line:

$$f_i = e_{ikl}\tau_k\sigma_{lm}b_m, \qquad (1)$$

where e_{ikl} is the Levi-Civita symbol (antisymmetric Kronecker symbol); τ_k are the components of the unit vector of the tangent to the dislocation line; σ_{lm} – components of the tensor of mechanical stresses external toward the dislocation; b_m – components of the dislocation Burgers vector. This expression applies Einstein's rule for summation using paired (occurring twice) indices. Indices can take on the values {x, y, z}.

As a result, the superposition of the components of the Peach-Keller force affecting the individual sections of the upcoming dislocation loop along the OY axis gives the expression:

$$F_y = -b^2 B \frac{h\left(3d^2+h^2\right)}{\left(d^2+h^2\right)^2} L, \qquad B = \frac{\mu}{2\pi\left(1-\sigma\right)}, \qquad (2)$$

where b is the modulus of the Burgers vector of the dislocation loop; μ is the shear modulus of the sample material; σ is the Poisson's ratio of the sample material; h is

the size of the dislocation loop along the OY axis; d is the distance between the head and the upcoming dislocation loops; L is the size of the dislocation loop along the OZ axis.

Thus, it becomes possible for the upcoming dislocation loop to shift in the negative direction of the OY axis. After the upcoming dislocation loop descends below the ZOX face, the component of the Peach-Keller force will affect section (1-2) of the dislocation loop in the negative direction of the OY axis.

$$F_y^{(1-2)} = -b^2 B \frac{(h+y_0)\left[3d^2 + (h+y_0)^2\right]}{\left[d^2 + (h+y_0)^2\right]^2} L, \quad (3)$$

where y_0 is the modulus of the distance from section (3-4) of the upcoming dislocation loop to the ZOX face.

The component of the Peach-Keller force will affect section (3-4) of the dislocation loop in the positive direction of the OY axis:

$$F_y^{(3-4)} = b^2 B \frac{y_0\left(3d^2 + y_0^2\right)}{\left(d^2 + y_0^2\right)^2} L. \quad (4)$$

If the condition is met

$$F_y^{(1-2)} + F_y^{(3-4)} = 0. \quad (5)$$

The upcoming dislocation loop will stop at a distance y_0 below the ZOX face. It will enter the slip system, without the obstacle in the form of the head loop of the cluster, and under the influence of the next upcoming dislocation loop, it will be able to continue sliding in it until it reaches the sample surface.

In the initial slip system, the place of the upcoming dislocation loop, which "dived" under the head dislocation loop, will be taken by the next dislocation loop of the cluster. It will repeat the described "diving" process twice and will also come to the surface of the sample.

A similar displacement will be performed by the next upcoming dislocation loop, and so on.

Under the condition of constant action of the source of dislocation loops [36], periodic areas of inhomogeneous deformation are formed on the sample surface, caused by the periodic elastic field of the system of dislocation loops, which partially emerged on the sample surface and fixed on it (Fig. 4a). Another option may be the formation of nanorelief in the form of periodic parallel steps (Fig. 4b).

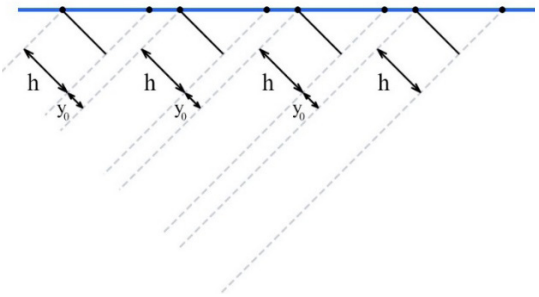

a)

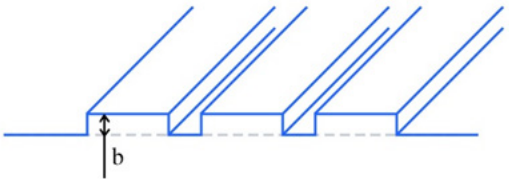

b)

Fig. 4. A system of dislocation loops fixed on the sample surface (a) and Periodic nano-steps on the sample surface (b).

The length of the nanosteps is equal to the length L of sections (1-2) and (3-4) of dislocation loops parallel to the OZ axis.

Let us find the value y_0 to estimate the distance between the nanosteps on the sample surface.

An attempt to directly solve Eq. (5) leads to an algebraic equation of the sixth degree. Its numerical coefficients depend on h and d – the values of the geometric parameters of the accumulation of dislocation loops. This makes it impossible to obtain a general analytical solution that demonstrates the relationship of these parameters in a general way. For each specific set of numerical values of the parameters, a numerical solution is possible.

There is another way to make an overall estimate of the value of y_0. To perform this estimate, we investigate the general expression for the Peach-Keller force acting on the sections of the dislocation loop parallel to the OZ axis:

$$F(y) = \pm b^2 B \frac{y\left(3d^2 + y^2\right)}{\left(d^2 + y^2\right)^2} L, \qquad (6)$$

where y is the ordinate of a section of the dislocation loop parallel to the OZ axis. The plus or minus sign is selected depending on the direction of the dislocation line.

The function $F(y)$ has two extreme points:

$$y_1 = \sqrt{\left(2\sqrt{3} - 3\right)} d \approx 0,681d ;$$

$$y_2 = -\sqrt{\left(2\sqrt{3} - 3\right)} d \approx -0,681d .$$

Taking into account the signs of expressions (3) and (4), we determine that at the points with ordinates y_2 the component $F^{(1-2)}$ has a maximum, and the component $F^{(3-4)}$ has a minimum. Thus, it can be estimated that, for all units

$$y_0 = 0,681d - \frac{h}{2}, \qquad (7)$$

the dislocation loop will be in a state of stable equilibrium relative to the displacement along the OY axis (Fig. 5).

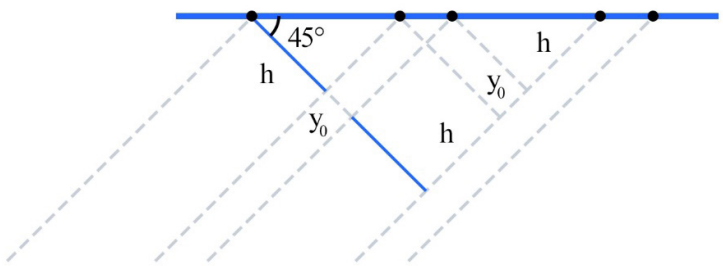

Fig. 5. Position of the upcoming dislocation loop after "diving" under the head loop, before reaching the sample surface.

Since the slip planes and the sample surface form an angle of 45°, the distance between adjacent parallel nanosteps can be estimated as:

$$l = \sqrt{2}y_0 = \sqrt{2}\left(0,681d - 0,5h\right). \qquad (8)$$

If there are no other defects in the crystal lattice of the sample, except for the accumulation of dislocation loops in their common slip system (Fig. 3a), then the superposition of the components of the Peach-Keller force displacing the loop along the OZ axis is zero.

In the presence of other defects in the bulk of the sample, or on its surface, the symmetry of the mutual arrangement of the head and upcoming dislocation loops will be violated. Such violation can lead to a nonzero superposition of the components of the Peach-Keller force displacing the loop along the OZ axis. In the simplest case, the initial relative displacement of the head and upcoming loops along the OZ axis is sufficient for this (Fig. 4a).

Thus, we can explain the longitudinal displacement of the nanowires observed on the sample surface after etching. The displacement of the upcoming dislocation loops in the ZOY face is carried out due to the shift and stops after the loop partially emerges onto the sample surface (Fig. 5). Accordingly, it is reasonable to assume that the value of the longitudinal displacement (along the OZ axis) for the incident dislocation loop *SS* will be close to the displacement along the OY axis and along the OX axis (Fig. 6):

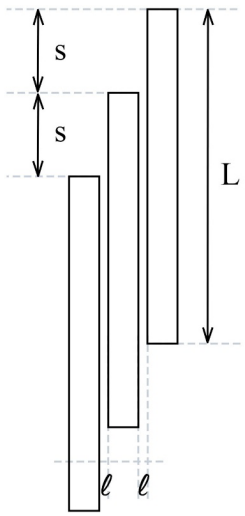

Fig. 6. Relative displacement of the head and upcoming dislocation loops along the OZ axis.

$$S = 2\left(h + y_0\right) = 2\left(0,5h + 0,681d\right). \quad (9)$$

Taking into account the fact that the cut-off radius of the elastic fields of the head dislocation loop, which partially emerged on the surface of the sample, is approximately equal to h, we take $d \approx h$ for a numerical estimate using Eqs. (8) and (9).

In this case, we get:

$$l \approx 0,256h\ ;\ S \approx 2,362h\ . \quad (10)$$

These estimates correspond closely to the experimental results shown in Fig. 1.

CONCLUSIONS

1. The paper demonstrates the possibility of forming specific nanostructures of the "parquet" type of nanowires on the InP surface. Their morphological and chemical parameters have been studied.
2. According to the results of scanning electron microscopy, it has been found that the thickness of each wire is about 10 microns, the height is up to 10 microns, and the length is between 100 and 130 microns. The distance between the parquet layers is 20 to 50 microns.
3. EDAX shows an excess of indium in the periodic oxide layers. The shift in stoichiometry toward excess indium is explained by the faster etching of the phosphorus sublattice.

The resulting nanostructure is characterised by an ordered transverse and longitudinal relative displacement of individual nanowires. A dislocation model is proposed to explain the mechanism of formation of such structure. The numerical estimates of the geometric parameters of the nanostructure obtained during theoretical modelling are adequate for the experimental results.

ACKNOWLEDGMENTS

The study has been supported by the Ministry of Education and Science of Ukraine via Project No. 0122U000129 "The Search for Optimal Conditions for Nanostructure Synthesis on the Surface of A3B5, A2B6 Semiconductors and Silicon for Photonics and Solar Energy". In addition, the research of A.I.P. and Y.S. has been partly supported by COST Action CA20129 "Multiscale Irradiation and Chemistry Driven Processes and Related Technologies" (MultiChem). Furthermore, A.I.P. also thanks HORIZON 2020 RISE-RADON Project "Irradiation Driven Nanofabrication: Computational Modelling Versus Experiment" for partial support.

REFERENCES

1. Monaico, E., Tiginyanu, I., & Ursaki, V. (2020). Porous Semiconductor Compounds. *Semiconductor Science and Technology*, 35 (10), 103001. doi: 10.1088/1361-6641/ab9477
2. Deng, T., Li, M., Wang, Y., & Liu, Z. (2015). Development of Solid-State Nanopore Fabrication Technologies. *Science Bulletin*, 60 (3), 304–319. doi: 10.1007/s11434-014-0705-8

3. Dolgyi, A., Bandarenka, H., Prischepa, S., Yanushkevich, K., Nenzi, P., Balucani, M., & Bondarenko, V. (2012). Electrochemical Deposition of Ni into Mesoporous Silicon. *ECS Transactions*, *41* (35), 111.
4. Shimanovich, D. L., Vorobjova, A. I., Tishkevich, D. I., Trukhanov, A. V., Zdorovets, M. V., & Kozlovskiy, A. L. (2018). Preparation and Morphology-Dependent Wettability of Porous Alumina Membranes. *Beilstein Journal of Nanotechnology*, *9* (1), 1423–1436.
5. He, Y., Tsutsui, M., Zhou, Y., & Miao, X. S. (2021). Solid-State Nanopore Systems: From Materials to Applications. *NPG Asia Materials*, *13* (1), 1–26. DOI: 10.1038/s41427-021-00313-z
6. Plesa, C., Verschueren, D., Pud, S., Van Der Torre, J., Ruitenberg, J. W., Witteveen, M. J., ... & Dekker, C. (2016). Direct Observation of DNA Knots Using a Solid-State Nanopore. *Nature Nanotechnology*, *11* (12), 1093–1097. DOI: 10.1038/nnano.2016.153
7. Zavatski, S., Popov, A. I., Chemenev, A., Dauletbekova, A., & Bandarenka, H. (2022). Wet Chemical Synthesis and Characterization of Au Coatings on Meso- and Macroporous Si for Molecular Analysis by SERS Spectroscopy. *Crystals*, *12* (11), 1656.
8. Ochs, D., Brause, M., Krischok, S., Stracke, P., Maus-Friedrichs, W., Puchin, V., ... & Kempter, V. (1998). Characterization of LiF and CaF2 Surfaces Using MIES and UPS (HeI). *Journal of Electron Spectroscopy and Related Phenomena*, *88*, 725–732.
9. Kozlovskiy, A., Kenzhina, I., Kaikanov, M., Stepanov, A., Shamanin, V., Zdorovets, M., & Tikhonov, A. (2018). Effect of Electronic Modification on Nanostructures Stability to Degradation. *Materials Research Express*, *5* (7), 075010.
10. Suchikova, Y., Kovachov, S., Bohdanov, I., Karipbaev, Z. T., Pankratov, V., & Popov, A. I. (2023). Study of the Structural and Morphological Characteristics of the CdxTeyOz Nanocomposite Obtained on the Surface of the CdS/ZnO Heterostructure by the SILAR Method. *Applied Physics A*, *129* (7), 499.
11. Suchikova, Y., Kovachov, S., Bohdanov, I., Popova, E., Moskina, A., & Popov, A. (2023). Characterization of CdxTeyOz/CdS/ZnO Heterostructures Synthesized by the SILAR Method. *Coatings*, *13* (3), 639.
12. Usseinov, A.B.; Akilbekov, A.T.; Kotomin, E.A.; Karipbayev, Z.T. (2019). The First Principles Calculations of CO_2 Adsorption on (1010) ZnO Surface. *AIP Conf. Proc.*, *2174*, 020181.
13. Klym, H., Ingram, A., Hadzaman, I., Karbovnyk, I., Vasylchyshyn, I., & Popov, A. I. (2019). Nanoporous Characterization of Modified Humidity-Sensitive MgO-Al2O3 Ceramics by Positron Annihilation Lifetime Spectroscopy Method. *IOP Conference Series: Materials Science and Engineering*, *503* (1), 012019.
14. Žalga, A., Abakevičienė, B., Žarkov, A., Beganskienė, A., Kareiva, A., & Tamulevičius, S. (2011). On the Properties of Yttria-Stabilized Zirconia Thin Films Prepared by Sol-Gel Method. *Medziagotyra*, *17* (2), 191–196.
15. Villarroel, R., Espinoza-Gonzalez, R., Lisoni, J., & Gonzalez-Moraga, G. (2018). Influence of the Oxygen Consumption on the Crystalline Structure of Titanium Oxides Thin Films Prepared by DC Reactive Magnetron Sputtering. *Vacuum, 154*, 52–57. doi: https://doi.org/10.1016/j.vacuum.2018.04.049
16. Suzuki, K., Sato, S., & Fujita, M. (2010). Template Synthesis of Precisely Monodisperse Silica Nanoparticles within Self-Assembled Organometallic Spheres. *Nature Chemistry*, *2* (1), 25–29. doi: 10.1038/nchem.446
17. Wei, C., Wu, G., Yang, S., & Liu, Q. (2016). Electrochemical Deposition of Layered Copper Thin Films Based on the Diffusion Limited Aggregation. *Scientific Reports*, *6* (1), 1–7. doi: 10.1038/srep34779
18. Ivanou, D. K., Streltsov, E. A., Fedotov, A. K., Mazanik, A. V., Fink, D., & Petrov, A. (2005). Electrochemical Deposition of PbSe and CdTe Nanoparticles onto p-Si (100) Wafers and into Nanopores in SiO_2/Si (100) Structure. *Thin Solid Films*, *490* (2), 154–160. doi: 10.1016/j.tsf.2005.04.046

19. Suchikova, Y.A., Kidalov, V.V., & Sukach, G.A. (2010). Influence of the Carrier Concentration of Indium Phosphide on the Porous Layer Formation. *Journal of Nano- and Electronic Physics*, *2* (4), 75–81.
20. Sato, T., Zhang, X., Ito, K., Matsumoto, S., & Kumazaki, Y. (2016). Electrochemical Formation of N-Type GaN and N-Type InP Porous Structures for Chemical Sensor Applications. *2016 IEEE Sensors,* (1–3). IEEE. doi: 10.1109/ICSENS.2016.7808443
21. Lee, E., Menumerov, E., Hughes, R. A., Neretina, S., & Luo, T. (2018). Low-Cost Nanostructures from Nanoparticle-Assisted Large-Scale Lithography Significantly Enhance Thermal Energy Transport across Solid Interfaces. *ACS Applied Materials & Interfaces*, *10* (40), 34690–34698. doi: 10.1021/acsami.8b08180
22. Monaico, E., Monaico, E. I., Ursaki, V. V., Tiginyanu, I. M., & Nielsch, K. (2019). Electrochemical Deposition by Design of Metal Nanostructures. *Surface Engineering and Applied Electrochemistry*, *55* (4), 367–372. doi: 10.3103/S1068375519040070
23. Suchikova, Y., Vambol, S., Vambol, V., & Mozaffari, N. (2019). Justification of the Most Rational Method for the Nanostructures Synthesis on the Semiconductors Surface. *Journal of Achievements in Materials and Manufacturing Engineering*, *92* (1–2), 19–28. doi: 10.5604/01.3001.0013.3184
24. Šimkiene, I., Kindurys, A., Treideris, M., & Sabataityte, J. (2008). Formation of Porous n-A_3B_5 Compounds. *Acta. Phys. Pol. A*, *3* (113), 1085–1090.
25. Delimitis, A., Komninou, P., Kehagias, T., Pavlidou, E., Karakostas, T., Gladkov, P., & Nohavica, D. (2008). Controlled Growth of Porous Networks in Phosphide Semiconductors. *Journal of Porous Materials*, *15* (1), 75–81. doi: 10.1007/s10934-006-9054-6
26. Ben Amara, E., Lebib, A., & Beji, L. (2020). Structural and Electrical Investigation of Porous GaAs Layers on Different Crystallographically Oriented GaAs Substrates. *Journal of Electronic Materials*, *49* (9), 5281–5292. doi: 10.1007/s11664-020-08294-5
27. Weng, Z., Chai, X., Liu, L., Li, L., Xu, H., Song, Z., & Liang, K. (2017). Effects of Temperature and Current Density on the Porous Structure of InP. *Journal of Solid State Electrochemistry*, *21*, 545–553. doi: 10.1007/s10008-016-3387-0
28. Praveenkumar, S., Lingaraja, D., Mathi, P. M., & Ram, G. D. (2019). An Experimental Study of Optoelectronic Properties of Porous Silicon for Solar Cell Application. *Optik*, *178*, 216–223. doi: 10.1016/j.ijleo.2018.09.176
29. Gerngross, M. D., Carstensen, J., & Föll, H. (2012). Electrochemical and Galvanic Fabrication of a Magnetoelectric Composite Sensor Based on InP. *Nanoscale Research Letters*, *7* (1), 1–5. doi: 10.1186/1556-276X-7-379
30. Korotcenkov, G., & Cho, B. K. (2010). Porous Semiconductors: Advanced Material for Gas Sensor Applications. *Critical Reviews in Solid State and Materials Sciences*, *35* (1), 1–37. doi: 10.1080/10408430903245369
31. Suchikova, J.A. (2015). Synthesis of Indium Nitride Epitaxial Layers on a Substrate of Porous Indium Phosphide. *Journal of Nano- and Electronic Physics*, *7* (3), 03017.
32. Cheng, H., Xiao, R., Bian, H., Li, Z., Zhan, Y., Tsang, C. K., ... & Li, Y. Y. (2014). Periodic Porous Silicon Thin Films with Interconnected Channels as Durable Anode Materials for Lithium Ion Batteries. *Materials Chemistry and Physics*, *144* (1–2), 25–30. doi: 10.1016/j.matchemphys.2013.12.003
33. Schmuki, P., Erickson, L. E., & Lockwood, D. J. (1998). Light Emitting Micropatterns of Porous Si Created at Surface Defects. *Physical Review Letters*, *80* (18), 4060. doi: 10.1103/PhysRevLett.80.4060
34. Suchikova, J.A., Kidalov, V.V., & Sukach, G.A. (2009). Blue Shift of Photoluminescence Spectrum of Porous InP. *ECS Transactions*, *25* (24), 59–64. doi: 10.1149/1.3316113

35. Vambol, S., Bogdanov, I., Vambol, V., Suchikova, Y., Kondratenko, O., Hurenko, O., & Onishchenko, S. (2017). Research into Regularities of Pore Formation on the Surface of Semiconductors. *Eastern-European Journal of Enterprise Technologies*, *3* (5–87), 37–44. doi: 10.1134/S1063782611010192
36. Yana, S. (2016). Porous Indium Phosphide: Preparation and Properties. *Handbook of Nanoelectrochemistry: Electrochemical Synthesis Methods, Properties, and Characterization Techniques*, 283–306. doi: 10.1007/978-3-319-15266-0_9
37. Lazarenko, A.S., Mikhailovskij, I.M., Rabukhin, V.B., & Velikodnaya, O.A. (1995). Nanotopography and Grain-Boundary Migration in the Vicinity of Triple Junctions. *Acta Metallurgica Et Materialia, 43* (2), 639–643. doi: 10.1016/0956-7151(94)00228-A
38. Suchikova, Y.A., Kidalov, V.V., & Sukach, G.A. (2011). Influence of Dislocations on the Process of Pore Formation in n-InP (111) Single Crystals. *Semiconductors*, *45* (1), 121–124. doi: 10.1134/S1063782611010192

Institute of Solid-State Physics, University of Latvia as the Centre of Excellence has received funding from the European Union's Horizon 2020 Framework Program H2020-WIDESPREAD-01–- 2016–2017-TeamingPhase2 under grant agreement No. 739508, project CAMART2.